Suppression of autophagy impedes glioblastoma development and induces senescence

Suppression of autophagy impedes glioblastoma development and induces senescence

Noor Gammoh[1#]*, Jane Fraser[1#], Cindy Puente[4], Heather M Syred[1], Helen Kang[4], Tatsuya Ozawa[2], Du Lam[3], Juan Carlos Acosta[1], Andrew J Finch[1], Eric Holland[2] and Xuejun Jiang[4]*

[1] Edinburgh Cancer Research UK Centre, Institute of Genetics and Molecular Medicine, University of Edinburgh, Edinburgh, EH4 2XR, UK.

[2] Division of Human Biology and Solid Tumor Translational Research (STTR), Fred Hutchinson Cancer Research Center, Seattle, WA 98109, USA.

[3] Celgene Corporation, 86 Morris Avenue, Summit, NJ 07901, USA.

[4] Cell Biology Program, Memorial Sloan Kettering Cancer Center, New York, NY 10065, USA.

* Corresponding authors:

Xuejun Jiang
Memorial Sloan Kettering Cancer Center, Box 522, 1275 York Avenue, New York, NY 10065 - USA
Email: jiangx@mskcc.org
Tel: +1 (212) 639 6814

Noor Gammoh
Edinburgh Cancer Research UK Centre, Institute of Genetics and Molecular Medicine, University of Edinburgh, Edinburgh, EH4 2XR - UK.
Email: noor.gammoh@igmm.ed.ac.uk
Tel: +44 (0)131 651 8526

[#] Equal contribution

Running Title: Autophagy is required for glioblastoma development

Keywords: ATG7, autophagy, brain, cancer, glioblastoma, metabolism, RCAS, senescence, tumor

Conflict of Interest and Financial Disclosure: None declared.

ABSTRACT

The function of macroautophagy/autophagy during tumor initiation or in established tumors can be highly distinct and context-dependent. To investigate the role of autophagy in gliomagenesis, we utilized a KRAS-driven glioblastoma mouse model in which autophagy is specifically disrupted via RNAi against *Atg7*, *Atg13* or *Ulk1*. Inhibition of autophagy strongly reduced glioblastoma development, demonstrating its critical role in promoting tumor formation. Further supporting this finding is the observation that tumors originating from *Atg7*-shRNA injections escaped the knockdown effect and thereby still underwent functional autophagy. In vitro, autophagy inhibition suppressed the capacity of *KRAS*-expressing glial cells to form oncogenic colonies or to survive low serum conditions. Molecular analyses revealed that autophagy-inhibited glial cells were unable to maintain active growth signaling under growth-restrictive conditions and were prone to undergo senescence. Overall, these results demonstrate that autophagy is crucial for glioma initiation and growth, and is a promising therapeutic target for glioblastoma treatment.

INTRODUCTION

Glioblastoma multiforme (GBM) is the most common adult brain tumor and one of the most aggressive cancers with a median survival of approximately one year.[1] Understanding survival response processes in GBM that contribute to its resistance would be crucial for therapy. One such survival process is autophagy, a cellular catabolic pathway frequently activated upon various stresses encountered by the cell including nutrient deprivation and hypoxia.[2]

During autophagy, cytoplasmic material is targeted for lysosomal degradation by a finely orchestrated series of vesicle formation and fusion events. A number of autophagy-essential protein complexes are required for the formation of a double-membrane structure, the phagohpore, that engulfs cytoplasmic materials, resulting in an enclosed vesicle called the autophagosome.[3] At the heart of the autophagy pathway lies a family of ubiquitin-like proteins, such as MAP1LC3/LC3 (microtubule-associated protein 1 light chain 3), essential for autophagosome maturation. Cytosolic LC3 (termed LC3-I) is recruited to the growing phagophore upon its ubiquitin-like conjugation to phosphatidylethanolamine forming LC3-II. This reaction is catalyzed by the activity of E1-, E2- and E3-like enzymes, which are ATG7, ATG3 and ATG12–ATG5-ATG16L1, respectively. Autophagy activation can be sensed by the ULK (unc-51 like kinase) signaling complex comprised of the protein kinase ULK1 and several regulatory components including ATG13 and RB1CC1/FIP200 (RB1-inducible coiled-coil 1).

Increasing evidence has demonstrated that autophagy is closely associated with cancer.[2,4] Autophagic degradation of cytoplasmic components can promote tumor cell survival

by providing nutrient supply, or can suppress tumorigenesis by clearing toxic cellular materials that can otherwise be carcinogenic. Such dual effects of autophagy on cancer progression are most likely dependent on the tumor type, genetic composition and stage. Genomic studies of GBM patient samples revealed mutations in multiple signaling pathways, including gain-of-function mutations in the receptor tyrosine kinase (RTK)-RAS-class I phosphoinositide 3-kinase oncogenic pathway,[5] which modulate autophagy.[6] Furthermore, in cultured GBM cells, autophagy is frequently activated as a stress response upon treatment with therapeutic agents.[7] However, how autophagy affects GBM development in vivo has not been addressed.

Cellular and xenograft experiments suggest an important role of autophagy in GBM.[8,9] However, these experiments utilize established GBM cell lines, and thus do not reflect the process of tumor initiation. For this reason, we aimed to inhibit autophagy along with oncogene activation in a genetically engineered mouse model. We used a Replication-Competent Avian Sarcoma-leukosis virus LTR splice acceptor/Tumor Virus A (RCAS/TVA) mouse model, which allows specific manipulation of genes of interest in glial progenitors. In this model, gliomagenesis is driven by oncogenic KRAS, and autophagy is specifically disrupted using shRNA sequences targeting *Atg7*, *Atg13* and *Ulk1*. Combined expression of the shRNA sequences and oncogene ensured inactivation of autophagy in tumor-forming cells. Unlike genetic deletion, which results in complete autophagy disruption, RNAi-mediated gene knockdown can more closely model the therapeutic situation by retaining residual activity of the target gene. Our results indicate that the autophagy inhibition strongly reduced GBM development in mice and abrogated the oncogenic potential of mutant *KRAS*-expressing glial cells ex vivo.

RESULTS AND DISCUSSION

RCAS/TVA mouse model for gliomagenesis.

In order to test the role of autophagy in GBM, we utilized the RCAS/TVA mouse model for gliomagenesis.[10] GBM is induced in *cdkn2a/ink4a-arf*$^{-/-}$ mice using RCAS viruses carrying oncogenic *KRAS* (*KRAS*^{G12D}). Intracranial injection of the virus-producing chicken fibroblast DF-1 cells into neonatal mice results in somatic gene transfer from the RCAS viruses to glial cells expressing the viral receptor, TVA, under the control of the *Nes/nestin* promoter (**Fig. 1A**). Importantly, tumors driven by *KRAS* expression using this model show a histopathology that closely mimics high-grade human tumors, including features such as pseudopalisading necrosis and microvascular proliferation.[11] The RCAS vectors were further modified to co-express shRNA sequences targeting autophagy-related (*Atg*) gene products along with *KRAS* expression to inhibit autophagy in tumor-initiating cells (such as *KRAS:shAtg7*, *KRAS:shAtg13* or *KRAS:shUlk1*) or control shRNA (*KRAS:shLacZ*). Using this system, efficient gene knockdown (**Fig. 1B**) and oncogene overexpression (**Fig. 1C**) can be achieved upon the infection of primary TVA-expressing glial cells (termed XFM cells) derived from uninjected mice.[12] Furthermore, shRNA-mediated inhibition of *Atg7*, *Atg13* or *Ulk1* resulted in autophagy inhibition as assessed by endogenous LC3 lipidation, but maintained residual autophagic activity (**Fig. 1D**).

Autophagy is required for GBM development.

To test the effect of autophagy inhibition on *KRAS*-mediated gliomagenesis, we performed intracranial injection of DF-1 cells expressing RCAS viruses into neonate mice.

Injection of DF-1 expressing *KRAS:shLacZ* RCAS viruses resulted in tumor formation in approximately 60% of the mice within 6 weeks after injection (**Fig. 2A-B**) as reported previously.[13] In contrast, the expression of shRNA targeting autophagy genes resulted in a dramatic reduction in *KRAS*-mediated tumor development (*KRAS:shAtg7*, ~10% of the injected mice developed tumors) or complete inhibition of tumor formation (*KRAS:shAtg13* and *KRAS:shUlk1*). Overall, these results indicate that autophagy is required for gliomagenesis induced by *KRAS* expression.

Having observed that some tumors did form in *KRAS:shAtg7*-injected mice (2 out of 21 mice), we assessed whether these tumors differed from the control (*KRAS:shLacZ*)-injected mice. We analyzed tissue sections by hematoxylin and eosin (H&E) staining and observed no difference in the tumor morphology between *KRAS:shLacZ* and *KRAS:shAtg7* tumors (**Fig. 2C**). Similarly, there was no difference in NES/nestin (marker of GBM) or MKI67/Ki67 (proliferation marker) staining (**Fig. 2D**). Next we examined whether *KRAS:shAtg7*-derived tumors exhibited efficient reduction of ATG7 protein levels. Interestingly, immunohistological staining showed comparable ATG7 levels between *shAtg7*- and *shLacZ*-expressing tumors, suggesting that the tumor cells bypassed the *Atg7* shRNA effect (**Fig. 2E**). We further confirmed the specificity of the anti-ATG7 antibody by staining mouse embryonic fibroblasts (MEFs) derived from wild type or *atg7* knockout mice (**Fig. 2F**). Overall, these observations further support the conclusion that the expression of autophagy-essential genes is required for GBM formation in the KRAS-RCAS/TVA model.

Autophagy is required for KRAS-driven oncogenic growth of glial cells.

The lack of tumor formation upon RNAi-mediated inhibition of *Atg7*, *Atg13* or *Ulk1* suggests that autophagy is required for KRAS-driven gliomagenesis in vivo. However, these results do not distinguish whether the absence of autophagy impedes KRAS-induced transformation or growth of transformed cells. In order to understand the role of autophagy in gliomagenesis, we infected XFM glial cells (*cdkn2a/ink4a-arf*$^{-/-}$) with RCAS viruses co-expressing *KRAS* and shRNA against *LacZ*, *Atg7*, *Atg13* or *Ulk1* (as in **Fig. 1B**). We observed no growth defects upon autophagy inhibition in cells grown under normal culture conditions in monolayer. Interestingly, when cells were seeded in anchorage-independent conditions in soft agar, colony formation was strongly reduced in KRAS cells co-expressing shRNA targeting *Atg7*, *Atg13* or *Ulk1* compared to *KRAS:shLacZ* expressing cells (**Fig. 3A**). Therefore, autophagy appears to be critical for KRAS-driven glial transformation. Furthermore, we tested whether autophagy is required for clonogenic growth under suboptimal conditions by culturing cells in low serum (0.1% fetal bovine serum [FBS]), a condition mimicking poor angiogenic state in tumors. Under this condition, autophagy inhibition by *Atg7*-shRNA resulted in failure of clonogenic cell growth when cells were allowed to recover in full growth medium containing 10% FBS compared to control cells (**Fig. 3B-C**). Overall, these studies indicate that autophagy is required for both oncogenic transformation of *KRAS*-expressing glial cells and their sustained viability under stressful conditions associated with gliomagenesis.

We further tested the underlying mechanism for the lack of clonogenic growth in autophagy-inhibited cells by analyzing growth signaling and survival pathways. We observed neither morphological changes indicative of cell death induction in cells cultured under low-serum condition (0.1% FBS) nor CASP3/caspase-3 activation, indicating that the difference in

growth capacity was not due to apoptotic cell death (**Fig. 3D**). Next, we tested whether growth signaling pathways were impeded by *Atg7* knockdown. When grown in normal culture medium, the phosphorylation status of signaling factors AKT, MAPK1/ERK2-MAPK3/ERK1, and RPS6 was comparable in *KRAS:shLacZ*- and *KRAS:shAtg7*-expressing cells, indicating that autophagy was dispensable under this condition. Interestingly, under low-serum conditions, while *KRAS:shLacZ*-expressing cells could maintain modest levels of AKT, MAPK1/3 and RPS6 phosphorylation, *KRAS:shAtg7*-expressing cells were more susceptible to serum withdrawal (**Fig. 3E**). We further confirmed the role of autophagy in maintaining growth signaling by culturing cells in hypoxic conditions (a critical aspect of GBM). Autophagy was significantly induced in *KRAS:shLacZ* cells grown under low oxygen conditions (0.5% O_2, **Fig. 3F**). Importantly, both AKT and MAPK1/3 phosphorylation were significantly lower in *KRAS:shAtg7* cells compared to control cells, indicating that growth signaling under hypoxia was compromised in the absence of autophagy. In contrast, no significant effects were observed on RPS6 phosphorylation, suggesting that the MTOR (mechanistic target of rapamycin [serine/threonine kinase]) complex 1 (MTORC1) signaling pathway may be dispensable under these conditions. Overall, the above results strongly suggest that autophagy is required to maintain growth signaling pathways in cells deprived of growth factors or grown under hypoxia.

Autophagy inhibition induces senescence and reduces metabolic activity under low serum conditions.

We further sought to characterize the consequences of autophagy inhibition in cells grown under suboptimal culture conditions. Having observed that in the absence of autophagy

cells failed to recover after being cultured in low-serum media for 14 days (**Fig. 3B**), we examined whether cells underwent irreversible growth arrest. To do so, we measured senescence-associated β-galactosidase (SA-GLB1) activity as an assay for cellular senescence. As shown in **Fig. 4A**, autophagy inhibition resulted in a significant increase of senescent cells in *KRAS*-expressing XFM cells compared to control cells when grown in low serum for 7 and, to a lesser extent, 14 days. Similarly, BrdU incorporation assay showed a reduced proliferation rate in *Atg7*-knockdown cells compared to control cells after 7 days of serum starvation, but the rate became comparable at later time points (14 days, **Fig. 4B**). Consistent with these observations, we found that at various time points following serum starvation the dephosphorylation and thereby activation of RB1/p105 (retinoblastoma 1)[14,15] and cellular levels of CDKN1B/p27 as well as markers of the senescence-associated secretory phenotype including IL1B/IL-1β and IL6 were elevated in *KRAS:shAtg7* cells compared to *KRAS:shLacZ* cells (**Fig. 4C-D**). These results suggest that when autophagy is defective, cells are more prone to undergo senescence. Interestingly, under low serum conditions, activation of TRP53/p53 was not detected, suggesting that in this context senescence may occur independently of TRP53[16,17] (**Fig. 4C**). These observations highlight the importance of autophagy in maintaining cell cycle progression in culture following growth factors withdrawal in KRAS-transformed cells.

We further sought to measure whether the metabolic activity of *KRAS*-expressing cells differed in the absence of autophagy in growth-arrested cells during prolonged serum starvation (**Fig. 4E**). When cells were grown under normal growth conditions (10% FBS), there was no significant difference in glucose, glutamine and pyruvate consumption or lactate production between the 2 cell types (**Fig. 4F**). Under conditions of serum starvation, however,

uptake of these nutrients was markedly reduced in autophagy-deficient cells indicating that overall biosynthetic activity in these cells was lower. Lactate production was also lower in *KRAS:shAtg7*-expressing cells, indicating reduced aerobic glycolysis. Overall, these results indicate that autophagy acts as a stress response pathway and is required to bypass senescence and maintain metabolic activity in growth-arrested conditions.

In this study, we demonstrate that RNAi-mediated suppression of autophagy impedes tumor incidence in a KRAS-driven, RCAS/TVA GBM model. This is in agreement with previous studies where suppression of autophagy by genetic deletion restricts growth of KRAS- and BRAF-driven tumors of the lung, pancreas and skin.[18-20] Further supporting our findings is the observation that tumors developing from *KRAS:shAtg7* injections retain *Atg7* expression. Loss of RNAi repression effect may be due to either silencing of the shRNA expression or additional mutations that render resistance to the shRNA.

The RCAS/TVA mouse model is a unique system to study gliomagenesis based on somatic gene transfer (using RCAS viruses) into a specific cell type (engineered to express viral TVA receptor).[10] Unlike xenograft models that utilize established cancer cells, this genetically engineered mouse model allows for the assessment of tumor initiation in the presence of a functional immune system. In addition, xenograft experiments rely on the injection of a large number of cells into the recipient animals which differ considerably from the process of tumor development generally involving the transformation of a single or few cells.[21] Indeed, considerable differences are observed when assessing the role of autophagy in GBM using the RCAS/TVA mouse model presented here and previously published xenograft studies. Xenograft

studies using GBM cell lines show that autophagy inhibition cooperates with drug treatment to restrict cell growth but has no effect on tumor growth in the absence of treatment.[8,9] However, our studies indicate that autophagy inhibition in the absence of drug treatment can affect tumor development (**Fig. 2**). The differences between these results may be due to the presence of an intact immune response in the RCAS/TVA model. Furthermore, GBM cell lines may have acquired additional mutations during prolonged in vitro culture thereby altering their response to autophagy inhibition. Alternatively, it is possible that inhibition of autophagy after tumor formation (xenograft models) may impose different effects compared to autophagy inhibition in a tumor initiation model (RCAS/TVA model). Further studies are required to elucidate these differences.

How does autophagy inhibition suppress gliomagenesis? Autophagy may facilitate cellular changes that are required for KRAS-mediated transformation, including genomic instability, metabolic stress and lipid homeostasis resulting from *KRAS* expression.[19,22] Our cell culture-based studies indicate that autophagy can support the growth of *KRAS*-expressing glial cells in unfavorable conditions such as the absence of cell attachment or reduced growth factors, key hallmarks of cellular transformation. Molecularly, we found that when grown under growth restrictive conditions, autophagy-deficient cells were unable to maintain activated growth signaling and were prone to senescence, characterized by the activation of RB1 and increased levels of CDKN1B/p27 and markers of the senescence-associated secretory phenotype.[23-25] Interestingly, our results show that autophagy is also required to maintain metabolic activity in growth-arrested cells during prolonged growth factor withdrawal, consistent with previous publications.[18,26] A recent study suggests that maintaining glycolysis

enhances cell survival during mitotic arrest induced by *Cdc20* deletion.[27] This may imply that, in a similar fashion, the absence of glycolysis in autophagy-defective cells may contribute to their inability to proliferate when restimulated with full growth medium as observed in our system. It remains to be defined whether the role of autophagy in maintaining cell growth and metabolic activity is required for gliomagenesis *in vivo*. Mouse models allowing conditional autophagy inhibition after tumor establishment will be useful for this purpose.

Our study is the first to demonstrate the effect of autophagy inhibition by RNAi on gliomagenesis in a genetically engineered mouse model. A recent study showed that adult mice with conditional whole body deletion of *Atg7* live for 2-3 months due to selective tissue damage.[28] However, in this model, complete inhibition of autophagy in mice with lung tumors induces tumor regression within 5 weeks, suggesting that a therapeutic window exists and can be exploited.[28] Additionally, when autophagy is significantly inhibited but not completely ablated, an anti-tumorigenic effect could already be achieved, as demonstrated by RNAi-based autophagy inhibition in our GBM mouse models. A partially inhibited autophagy pathway is likely to maintain the homeostatic function of autophagy in normal tissues during prolonged treatment, thus avoiding the lethal effect of complete, whole body elimination of autophagy function.

MATERIALS AND METHODS

Cell culture and treatment.

DF-1 chicken fibroblasts (ATCC, CRL-12203) and glial cells derived from the RCAS mouse model expressing TVA receptor XFM,[12] were cultured in DMEM (Life Technologies, 41966029 supplemented with 10% FBS, L-glutamine (2 mM), penicillin (10 units/mL) and streptomycin (0.1 mg/ml).

For amino acid starvation experiments, cells were grown in DMEM lacking amino acids and serum for 2 h prior to harvest, as described previously.[29] The lysosomal inhibitor, bafilomycin A_1 (Sigma, B1793), was added as indicated at a final concentration of 20 nM for 2 h. Staurosporine (STS; Sigma, S5921) was added to cells for a final concentration of 1 μM for 16 h.

Western blot and antibodies.

For western blot analyses, cell lysates were prepared in RIPA buffer (10 mM Tris pH 7.4, 100 mM NaCl, 1 mM ethylenediaminetetraacetic acid, 1 mM ethylene glycol tetraacetic acid, 0.1% sodium dodecyl sulfate, 1% Triton-X100 [Sigma, T9284], 1 mM 2-mercaptoethanol, 0.5% sodium deoxycholate and 10% glycerol) and analyzed by SDS-PAGE as described previously.[7, 29] The following antibodies were used: anti-LC3 (Sigma, L7543); anti-ACTB/beta-actin (Sigma, A5316); anti-ULK1 (Sigma, A7481); anti-ATG7 (Santa Cruz Biotechnology, clone H300, sc-33211; or Sigma, A2856); anti-pan-RAS (EMD Millipore, OP40); anti-RAS G12D mutant specific (Cell Signaling Technology, 14429); anti-ATG13 (Sigma, SAB4200100); anti-TUBG/γ-tubulin (Sigma, GTU-88); anti-HIF1A/HIF1α (R&D Systems, MAB1536); anti-phosphorylated (p)-AKT (Ser473; Cell Signaling Technology, 4060); anti-total AKT (Cell Signaling Technology, 9272); anti-p-MAPK1/ERK2-MAPK3/ERK1 (Thr202/Tyr204; Cell Signaling Technology, 4370); anti-total MAPK1/ERK2-MAPK3/ERK1 (Cell Signaling Technology, 9102); anti-pRPS6/S6 (Ser235/236; Cell

Signaling Technology, 4858); anti-total RPS6/S6 (Cell Signaling Technology, 2217); anti-CASP3/caspase-3 (Cell Signaling Technology, 9665); anti-RB1/p105 (BD Biosciences, 554136); anti-TRP53/p53 (Cell Signaling Technology, 2524); anti-CDKN1B/p27 (Cell Signaling Technology, 2552); anti-IL6/interleukin 6 (R&D Systems, BAF-406); anti-IL1B/interleukin 1 beta (R&D Systems, AF-301-NA).

Injections.

All animal experiments were done in accordance with protocols approved by the Institutional Animal Care and Use Committees of Memorial Sloan Kettering Cancer Center and followed NIH guidelines for animal welfare. The RCAS/TVA system used in this work to induce gliomas in vivo in immunocompetent mice has been described previously.[30] *N/TVA;cdkn2a/ink4a-arf)*$^{-/-}$*;Pten*$^{fl/fl}$ mice were used for the RCAS mediated gliomagenesis in this study.[13] Briefly, DF-1 cells were transfected with the relevant RCAS viral plasmid using Lipofectamine2000 (Invitrogen, 11668019) according to the manufacturer's protocol. The cells were regularly maintained for at least 3 passages for propagation of the RCAS viruses to entire cells. Cells were then used for injection into murine brain. Newborn pups were injected intracranially with 1 µL of ~1x10^5 DF-1 cells. Then mice were monitored until they developed symptoms of GBM such as lethargy, poor grooming, weight loss, dehydration or macrocephaly. GBM incidence or absence was confirmed by H&E staining of brain sections in all injected animals. Kaplan-Meier analysis demonstrating symptom-free survival in murine gliomas was performed using the Prism software (GraphPad).

Vector constructs.

For the generation of the RCAS-shRNA vector, shRNAs were initially assembled in the pSUPER.retro vector (OligoEngine, VEC-PRT-0002). The shRNAs containing the *H1* promoter were PCR-amplified and then inserted into the RCAS-Y vector (generated and provided by Dr Yi Li, Baylor College of Medicine, Texas)[31] using NotI and PacI restriction sites. *KRAS* was subsequently cloned using NotI restriction sites. The shRNA target sequences are as follows: *Atg7* 5' CACATAGCATCATCTTTGA; *Atg13* 5' GAGAAGAATGTCCGAGAAT; *Ulk1* 5'GAGCAAGAGCACACGGAAA.

Immunocytochemistry.

Mouse brains harvested from animals were fixed in 10% formalin for 24-72 h and then transferred to 70% ethanol. Samples were then paraffin-embedded, sectioned and stained with H&E by Histoserv Inc, Maryland. Similarly, MEFs derived from wild-type or *atg7* knockout cells were pelleted and processed for paraffin embedding. For immunocytochemistry staining, paraffin-embedded sections were treated with xylene twice for 10 min each before being sequentially hydrated in decreasing concentrations of ethanol. Epitope retrieval was performed by incubating slides in 10 mM sodium citrate buffer, pH 6 for 15 min at 95°C then allowed to cool for 20-45 min. Subsequently, slides were blocked with TBST (150 mM NaCl and 10 mM Tris pH 7.5, 0.1% Tween 20 [Sigma, P5927] + 5% BSA [Thermo Fisher Scientific, BP1605-100]) for 45 min, and incubated with primary antibodies overnight at 4°C. Subsequently, slides were incubated with Alexa fluorescent secondary antibodies (Life Technologies, A-11012 and A-11032) and images acquired using a Nikon Eclipse Ti-U Confocal Microscope. The antibodies

used in this study are anti-ATG7 (Sigma, A2856), anti-MKI67/Ki67 (Vector Labs, VP-K451), and anti-NES/nestin (BD biosciences, 556309).

Colony formation assay.

XFM cells were seeded in 6-cm dishes; 24 h later cells were cultured in 0.1% FBS for 2 weeks (with medium replenished after 1 week) followed by growth in 10% FBS for a further 1 week. Cells were then fixed with 10% formaldehyde and stained with Giemsa (Sigma, GS500) to visualize colonies.

Hypoxia.

For hypoxia experiments, cells were incubated in a Whitley H35 Hypoxystation set to 37°C and 0.5% O_2. 72 h later, cells were lysed inside the Hypoxystation and analyzed by western blotting.

Soft agar assay.[32]

XFM cells were seeded at 10,000 cells/well in a 6-well dish. Cell suspension (final volume 1.5 mL) containing 0.4% low gelling agarose (Sigma, A4018) in full growth DMEM was overlaid with a layer of 0.5% agarose and left to solidify at 4°C. Cells were then incubated at 37°C, fed weekly with 0.4% agarose-containing DMEM and analyzed after ~3 weeks by staining with 0.02% Iodonitrotetrazolium chloride (Sigma, I10406). Colonies were quantified using an Optronix Gelcount (Oxford Optronix). All assays were conducted in triplicates in 3 independent experiments.

Senescence-associated β-galactosidase assay (SA-GLB1).[23]

Cellular senescence was measured using an SA-GLB1 assay. Briefly, cells were fixed with 0.5% glutaraldehyde then incubated with X-gal staining solution, pH 6.0 (1mM $MgCl_2$ phosphate-buffered saline [Fisher BioReagents, BP399], X-gal [Thermo Fisher Scientific, R0941], 0.12 mM $K_3Fe[CN]_6$ [Sigma, 60299], 0.12 mM $K_4Fe[CN]_6$ [Sigma, 60279]) overnight at 37°C. Images of cells were taken using a Nikon Digital Sight DS-L3.

BrdU incorporation assay.

For the BrdU incorporation assay, cells were pulsed with 50 µM BrdU (Sigma, B5002) for 18 h followed by fixation with 3.7% paraformaldehyde and permeabilization with 0.2% Triton-X100. Cells were blocked with 0.2% gelatin-fish (Sigma, G7765) in 5% BSA-phosphate-buffered saline and incubated with anti-BrdU primary antibody (1:2000; BD Biosciences, 555627), 0.5 U/L DNase (Sigma, D4527), and 1 mM $MgCl_2$ in blocking solution. Subsequently, slides were incubated with Alexa secondary antibodies (Life Technologies, A-11001) and 1 µg/ml DAPI; images were acquired using ImageXpress and analyzed using MetaXpress software.

Metabolite measurement.

XFM cells were grown in 0.1% FBS for 2 weeks and fresh 0.1% FBS medium was added and cells grown for a further 3 or 5 days. Alternatively, cells grown in 10% FBS were analyzed after 3 days of culture. Metabolites were extracted from the medium using ice-cold extraction buffer (50% methanol, 30% acetonitrile). Extracted metabolites were separated on a Zic-pHILIC column (Merck Millipore) using a Thermo Ultimate BioRS HPLC with a single step linear gradient of 10%-95% A over 20 min (mobile phases were [A] 20 mM ammonium carbonate [B] acetonitrile). Metabolites were eluted into a Q-Exactive mass spectrometer (Thermo Fisher

Scientific) using a flow rate of 300 µl/min. Metabolite masses were acquired in negative mode within the range of 78-250 m/z. Relative metabolite abundance was then determined by integrating the ion peak area (Quan Thermo Xcalibur) and normalized to cell number.

Statistical analyses.

All data are presented as the mean ± SEM. The statistical significance was evaluated using two-tailed, unpaired student's t-test. Percentage tumor-free survival Kaplan Meier curve was analyzed using Log-rank Mantel-Cox test (Graphpad Prism software). The data were considered significant when the P value was less than 0.05 (*).

LIST OF ABBREVIATIONS

ATG	autophagy-related
FBS	fetal bovine serum
GBM	glioblastoma multiforme
H&E	hematoxylin and eosin
KRAS	Kirsten rat sarcoma viral oncogene homolog
MAP1LC3/LC3	microtubule-associated protein 1 light chain 3 (MAP1LC3)
MEFs	mouse embryonic fibroblasts

RCAS	replication-competent avian sarcoma-leukosis virus LTR splice acceptor/tumor virus A
SA-GLB1	senescence-associated galactosidase, beta 1
ULK1	unc-51 like kinase 1

ACKNOWLEDGEMENTS

We would like to thank members of the Jiang and Gammoh laboratories for helpful discussions. This work was supported in part by a Goodwin Experimental Therapeutic Center fund, a Cycle for Survival fund, and NIH R01CA166413 and R01GM113013 (to X.J.) as well as an NIH fellowship 1F32CA162691 and a Carnegie Trust for the Universities of Scotland Grant (to N.G.).

REFERENCES

1. Huse JT, Holland E, DeAngelis LM. Glioblastoma: molecular analysis and clinical implications. Annual review of medicine 2013; 64:59-70.
2. White E. Deconvoluting the context-dependent role for autophagy in cancer. Nature reviews 2012; 12:401-10.
3. Klionsky DJ, Schulman BA. Dynamic regulation of macroautophagy by distinctive ubiquitin-like proteins. Nat Struct Mol Biol 2014; 21:336-45.
4. Gammoh N, Wilkinson S. Autophagy in cancer biology and therapy. Frontiers in Biology 2014; 9:35–50.
5. Verhaak RG, Hoadley KA, Purdom E, Wang V, Qi Y, Wilkerson MD, et al. Integrated genomic analysis identifies clinically relevant subtypes of glioblastoma characterized by abnormalities in PDGFRA, IDH1, EGFR, and NF1. Cancer Cell 2010; 17:98-110.
6. Schmukler E, Kloog Y, Pinkas-Kramarski R. Ras and autophagy in cancer development and therapy. Oncotarget 2014; 5:577-86.
7. Gammoh N, Lam D, Puente C, Ganley I, Marks PA, Jiang X. Role of autophagy in histone deacetylase inhibitor-induced apoptotic and nonapoptotic cell death. Proc Natl Acad Sci U S A 2012; 109:6561-5.
8. Fan QW, Cheng C, Hackett C, Feldman M, Houseman BT, Nicolaides T, et al. Akt and autophagy cooperate to promote survival of drug-resistant glioma. Sci Signal 2010; 3:ra81.
9. Hu YL, DeLay M, Jahangiri A, Molinaro AM, Rose SD, Carbonell WS, et al. Hypoxia-induced autophagy promotes tumor cell survival and adaptation to antiangiogenic treatment in glioblastoma. Cancer Res 2012; 72:1773-83.
10. Hambardzumyan D, Amankulor NM, Helmy KY, Becher OJ, Holland EC. Modeling Adult Gliomas Using RCAS/t-va Technology. Transl Oncol 2009; 2:89-95.
11. Uhrbom L, Kastemar M, Johansson FK, Westermark B, Holland EC. Cell type-specific tumor suppression by Ink4a and Arf in Kras-induced mouse gliomagenesis. Cancer Res 2005; 65:2065-9.
12. Dai C, Celestino JC, Okada Y, Louis DN, Fuller GN, Holland EC. PDGF autocrine stimulation dedifferentiates cultured astrocytes and induces oligodendrogliomas and oligoastrocytomas from neural progenitors and astrocytes in vivo. Genes Dev 2001; 15:1913-25.
13. Uhrbom L, Dai C, Celestino JC, Rosenblum MK, Fuller GN, Holland EC. Ink4a-Arf loss cooperates with KRas activation in astrocytes and neural progenitors to generate glioblastomas of various morphologies depending on activated Akt. Cancer Res 2002; 62:5551-8.
14. Broude EV, Swift ME, Vivo C, Chang BD, Davis BM, Kalurupalle S, et al. p21(Waf1/Cip1/Sdi1) mediates retinoblastoma protein degradation. Oncogene 2007; 26:6954-8.
15. Ludlow JW, Shon J, Pipas JM, Livingston DM, DeCaprio JA. The retinoblastoma susceptibility gene product undergoes cell cycle-dependent dephosphorylation and binding to and release from SV40 large T. Cell 1990; 60:387-96.
16. Prieur A, Besnard E, Babled A, Lemaitre JM. p53 and p16(INK4A) independent induction of senescence by chromatin-dependent alteration of S-phase progression. Nat Commun 2011; 2:473.
17. Zou X, Ray D, Aziyu A, Christov K, Boiko AD, Gudkov AV, et al. Cdk4 disruption renders primary mouse cells resistant to oncogenic transformation, leading to Arf/p53-independent senescence. Genes Dev 2002; 16:2923-34.
18. Yang S, Wang X, Contino G, Liesa M, Sahin E, Ying H, et al. Pancreatic cancers require autophagy for tumor growth. Genes Dev 2011; 25:717-29.
19. Guo JY, Karsli-Uzunbas G, Mathew R, Aisner SC, Kamphorst JJ, Strohecker AM, et al. Autophagy suppresses progression of K-ras-induced lung tumors to oncocytomas and maintains lipid homeostasis. Genes Dev 2013; 27:1447-61.

20. Xie X, Koh JY, Price S, White E, Mehnert JM. Atg7 overcomes senescence and promotes growth of BRAFV600E-driven melanoma. Cancer Discov 2015.
21. Hambardzumyan D, Parada LF, Holland EC, Charest A. Genetic modeling of gliomas in mice: new tools to tackle old problems. Glia 2011; 59:1155-68.
22. Karantza-Wadsworth V, Patel S, Kravchuk O, Chen G, Mathew R, Jin S, et al. Autophagy mitigates metabolic stress and genome damage in mammary tumorigenesis. Genes Dev 2007; 21:1621-35.
23. Acosta JC, Banito A, Wuestefeld T, Georgilis A, Janich P, Morton JP, et al. A complex secretory program orchestrated by the inflammasome controls paracrine senescence. Nat Cell Biol 2013; 15:978-90.
24. Alexander K, Hinds PW. Requirement for p27(KIP1) in retinoblastoma protein-mediated senescence. Mol Cell Biol 2001; 21:3616-31.
25. Muñoz-Espín D, Serrano M. Cellular senescence: from physiology to pathology. Nat Rev Mol Cell Biol 2014; 15:482-96.
26. Guo JY, Chen HY, Mathew R, Fan J, Strohecker AM, Karsli-Uzunbas G, et al. Activated Ras requires autophagy to maintain oxidative metabolism and tumorigenesis. Genes Dev 2011; 25:460-70.
27. Doménech E, Maestre C, Esteban-Martínez L, Partida D, Pascual R, Fernández-Miranda G, et al. AMPK and PFKFB3 mediate glycolysis and survival in response to mitophagy during mitotic arrest. Nat Cell Biol 2015.
28. Karsli-Uzunbas G, Guo JY, Price S, Teng X, Laddha SV, Khor S, et al. Autophagy is required for glucose homeostasis and lung tumor maintenance. Cancer Discov 2014; 4:914-27.
29. Gammoh N, Florey O, Overholtzer M, Jiang X. Interaction between FIP200 and ATG16L1 distinguishes ULK1 complex-dependent and -independent autophagy. Nat Struct Mol Biol 2013; 20:144-9.
30. Hu X, Pandolfi PP, Li Y, Koutcher JA, Rosenblum M, Holland EC. mTOR promotes survival and astrocytic characteristics induced by Pten/AKT signaling in glioblastoma. Neoplasia 2005; 7:356-68.
31. Dong J, Tong T, Reynado AM, Rosen JM, Huang S, Li Y. Genetic manipulation of individual somatic mammary cells in vivo reveals a master role of STAT5a in inducing alveolar fate commitment and lactogenesis even in the absence of ovarian hormones. Dev Biol 2010; 346:196-203.
32. Sun Q, Overholtzer M. Methods for the study of entosis. Methods Mol Biol 2013; 1004:59-66.

FIGURE LEGENDS

Figure 1. RCAS mouse model for gliomagenesis. (**A**) Outline of the RCAS mouse model. RCAS viruses harboring an oncogenic *KRAS* gene and autophagy shRNA are amplified in chicken fibroblasts. Intracranial injection of the fibroblasts in neonatal mice expressing the viral receptor, TVA, under the control of the *Nes/nestin* promoter results in gene transfer from the RCAS vectors to glial progenitors. (**B**-**C**) Validation of the RCAS-mediated gene knockdown (**B**) and *KRAS* overexpression (**C**). Primary glial cells (XFM) expressing the viral receptor TVA harvested from uninjected mice were infected in culture with RCAS viruses expressing *KRAS* and the indicated shRNA. (**D**) Inhibition of autophagy in glial cells expressing *KRAS* in the presence of shRNA against *Atg7*, *Atg13 or Ulk1*. XFM cells were amino acid starved (AA starve) for 2 h in the presence or absence of bafilomycin A_1 (BafA1; 20 nM) to inhibit lysosomal degradation.

Figure 2. Autophagy is required for GBM development. Mice were injected with RCAS vectors expressing *KRAS* in the presence of shRNA against *LacZ*, *Atg7*, *Atg13 or Ulk1*. (**A**) Kaplan Meier curve measuring tumor-free animals monitored up to 10 weeks after injection with the indicated RCAS expressing cells. ***, $p<0.001$ (Log-rank Mantel-Cox test). (**B**) Animal numbers of those plotted in (**A**). (**C**) Representative H&E images of mouse brain sections showing GBM development in the indicated injections. (**D**) Tissue sections of normal or GBM brains were stained with antibodies to NES/nestin, or MKI67/Ki67 or with DAPI. (**E**) Immunocytochemical staining of brain sections using an antibody against ATG7. (**F**) Similar staining procedures using *atg7* knockout (KO) or wild-type (WT) MEF cells to confirmed antibody specificity.

Figure 3. Inhibition of autophagy suppresses oncogenic growth and growth signaling pathways in *KRAS*-expressing glial cells. Primary glial cells (XFM) were transduced with RCAS viruses co-expressing KRAS along with the indicated shRNA and grown under the indicated conditions. (**A**-**B**) Transduced XFM cells were grown in (**A**) soft agar or (**B**) low serum (0.1% FBS) for 2 weeks followed by incubation in full growth medium for 1 week. (**C**) Representative images of cell morphology for cells treated as in (**B**). (**D**) No induction of apoptosis was observed (measured by cleaved CASP3) in cells cultured in 0.1% FBS for the indicated time points. Staurosporine (STS) treatment in *KRAS:shLacZ* cells was used as a positive control for CASP3 activation. (**E**) Cells grown in low serum (0.1% FBS) for the indicated times and cell lysates were analyzed by western blot using antibodies against the indicated proteins. (**F**) *KRAS:shLacZ*- or *KRAS:shAtg7*-expressing XFM cells were grown under hypoxic conditions (0.5% O_2) for 72 h and cell lysates analyzed. Statistical analyses are shown of 3 independent experiments performed in triplicates including error bar (SEM values). *, $p<0.05$; **, $p<0.01$, ***, $p<0.001$ (student's t-test, unpaired two-tailed).

Figure 4. Autophagy is required for suppressing senescence and maintaining metabolism under low-serum conditions. (**A**) *KRAS:shLacZ*- or *KRAS:shAtg7*-expressing XFM cells were incubated in 0.1% serum for 7 or 14 days. Cells were fixed and SA-GLB1 activity was measured as an indicator of cellular senescence. Quantification of approximately 200 cells per condition of 3 independent experiments is shown with SEM values. Representative images are shown below. (**B**) BrdU incorporation assay of cells treated as in (**A**). Statistical analyses are shown of 3 independent experiments performed in triplicates including error bar (SEM values). (**C**-**D**) Western blot analyses of XFM cell lysates cultured in 10% FBS (day 0) or 0.1% FBS (3, 7 or 14

days). (**E**) Schematic presentation of the experimental outline used to analyze metabolites in tissue culture medium. Cells were cultured in 10% FBS and medium collected after 3 days (10%, Day 3). Alternatively, cells were cultured in 0.1% FBS for 14 days, fresh medium containing 0.1% FBS was added and medium was collected following a further 3 or 5 days of culture (0.1%, Day 3 or Day 5). (**F**) Ion count (i.c.) measurements of the indicated metabolites normalized to cell numbers in tissue culture medium using mass spectrometry of XFM cells grown as described in (**E**). *, $p<0.05$; **, $p<0.01$; ***, $p<0.001$, ns, nonspecific ($p>0.05$; student's t-test, unpaired two-tailed).

Figure 1

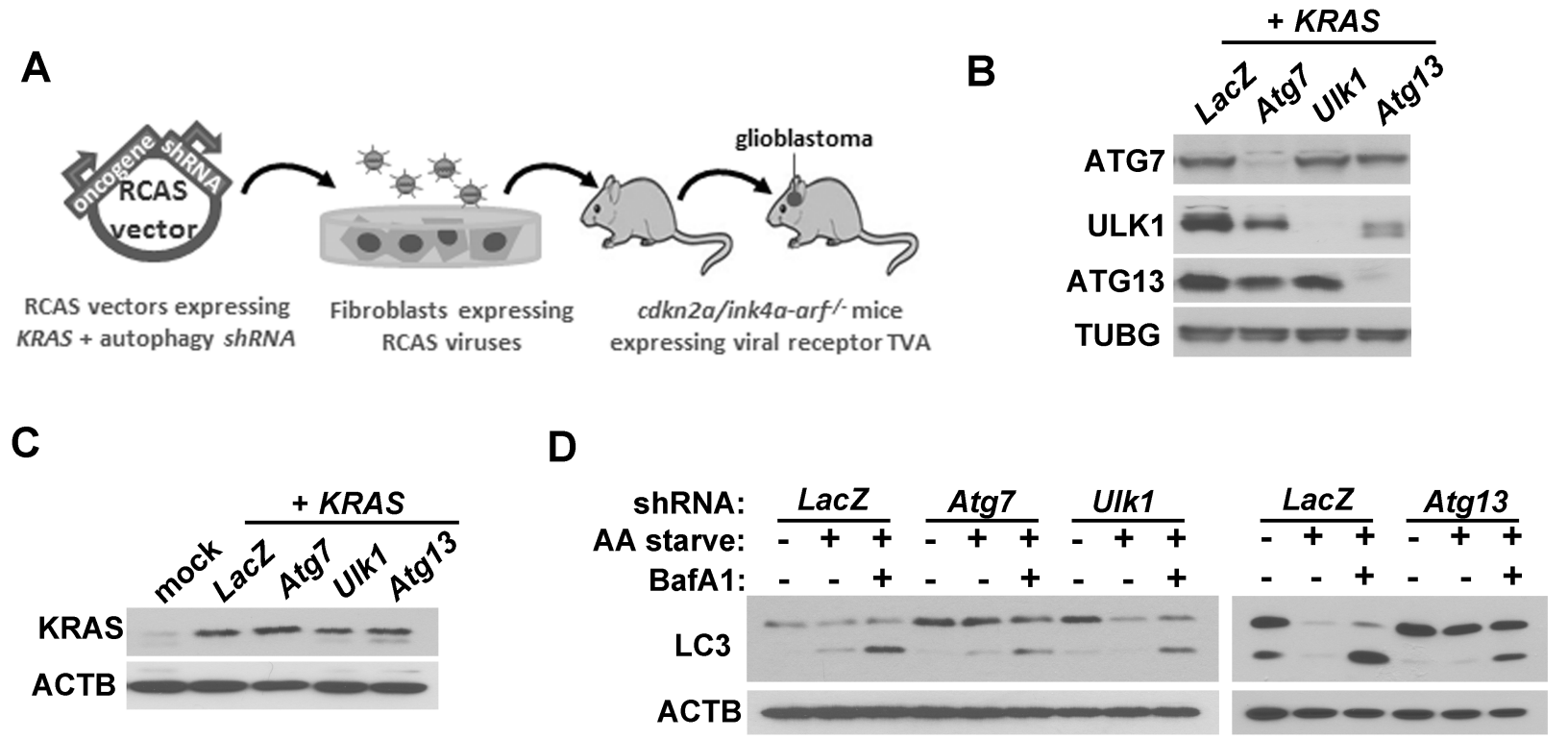
A
oncogene
shRNA
RCAS
vector
glioblastoma
RCAS vectors expressing
KRAS + autophagy shRNA
Fibroblasts expressing
RCAS viruses
cdkn2a/ink4a-arf-/- mice
expressing viral receptor TVA
B
+ KRAS
LacZ
Atg7
Ulk1
Atg13
ATG7
ULK1
ATG13
TUBG
C
+ KRAS
mock
LacZ
Atg7
Ulk1
Atg13
KRAS
ACTB
D
shRNA:
LacZ
Atg7
Ulk1
LacZ
Atg13
AA starve:
BafA1:
LC3
ACTB

Figure 2

A

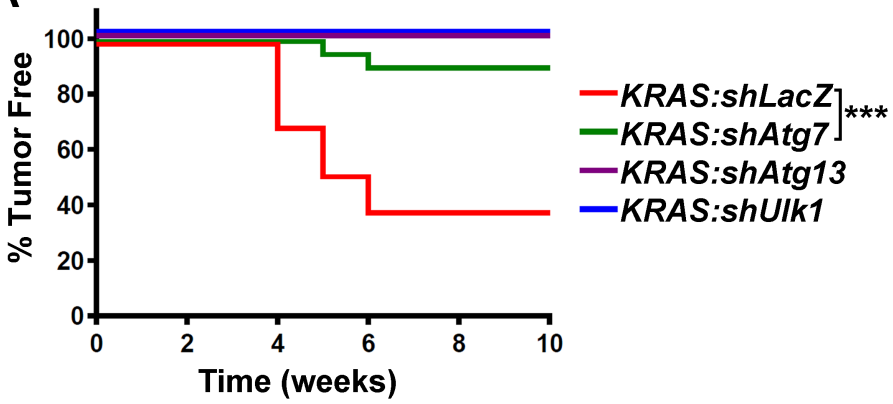

B

Injection	Positive tumors	Total injected	% tumors
KRAS:shLacZ	14	23	60.9%
KRAS:shAtg7	2	21	9.5%
KRAS:shAtg13	0	21	0%
KRAS:shUlk1	0	21	0%

C

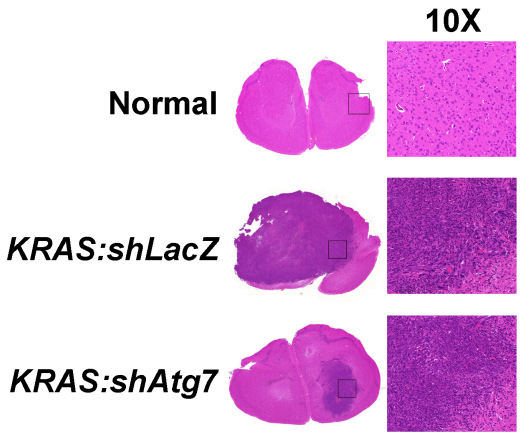

D

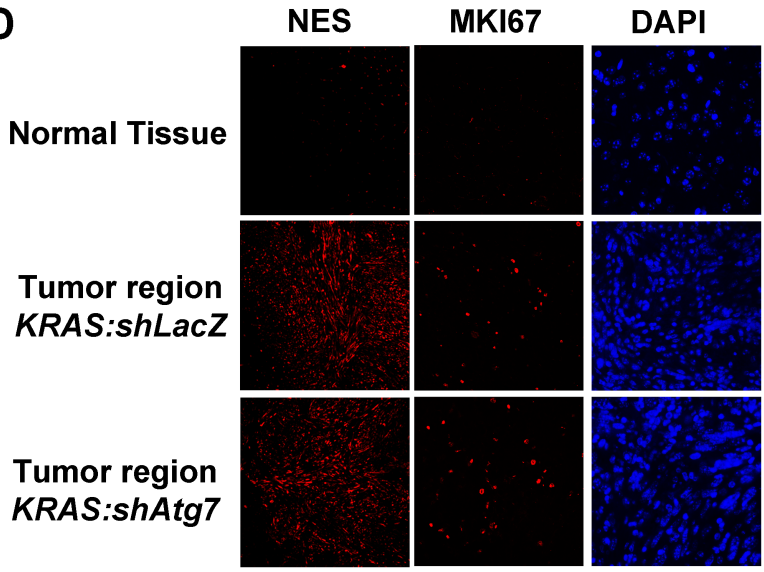

E

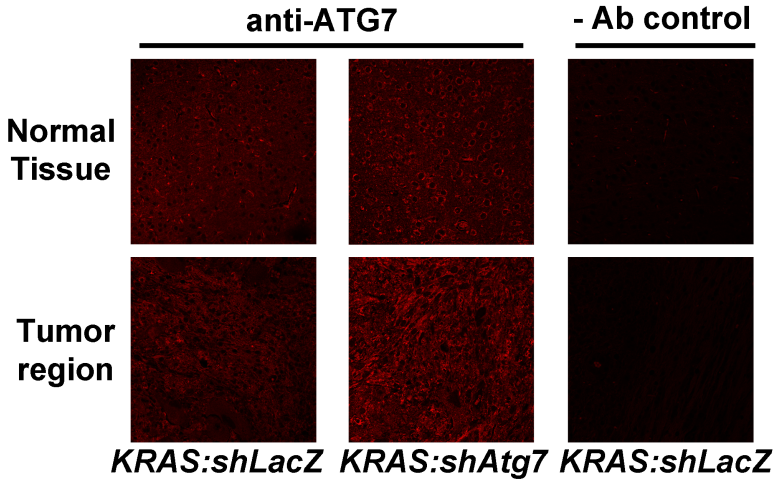

F

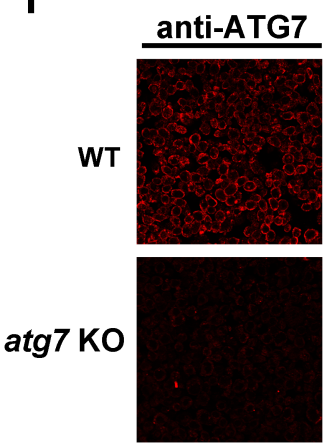

Figure 3

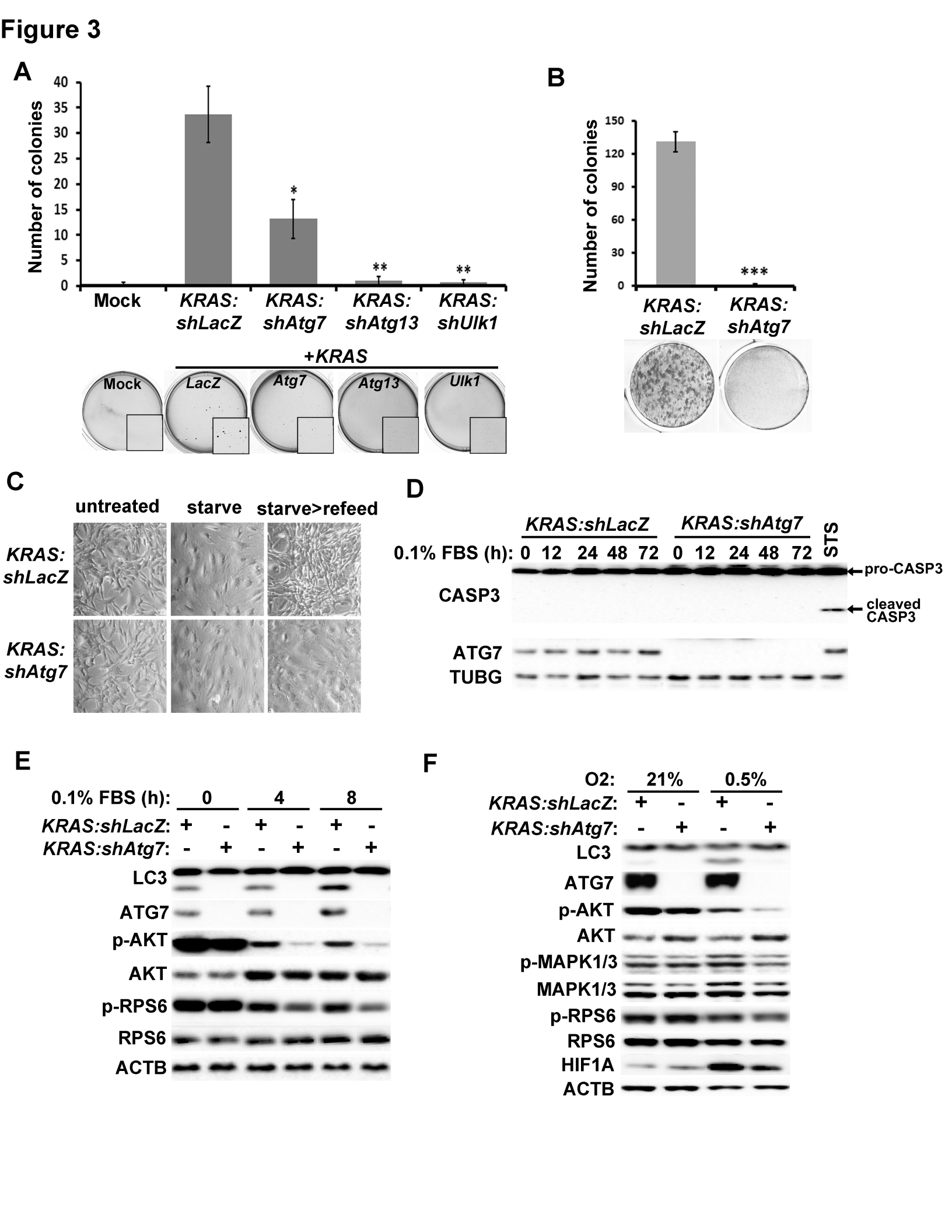
A
Number of colonies
40
35
30
25
20
15
10
5
0
*
**
**
Mock
KRAS: shLacZ
KRAS: shAtg7
KRAS: shAtg13
KRAS: shUlk1
+KRAS
Mock
LacZ
Atg7
Atg13
Ulk1
B
Number of colonies
150
120
90
60
30
0
***
KRAS: shLacZ
KRAS: shAtg7
C
untreated
starve
starve>refeed
KRAS: shLacZ
KRAS: shAtg7
D
KRAS:shLacZ
KRAS:shAtg7
STS
0.1% FBS (h): 0 12 24 48 72 0 12 24 48 72
pro-CASP3
cleaved CASP3
CASP3
ATG7
TUBG
E
0.1% FBS (h): 0 4 8
KRAS:shLacZ: + - + - + -
KRAS:shAtg7: - + - + - +
LC3
ATG7
p-AKT
AKT
p-RPS6
RPS6
ACTB
F
O2: 21% 0.5%
KRAS:shLacZ: + - + -
KRAS:shAtg7: - + - +
LC3
ATG7
p-AKT
AKT
p-MAPK1/3
MAPK1/3
p-RPS6
RPS6
HIF1A
ACTB

Figure 4

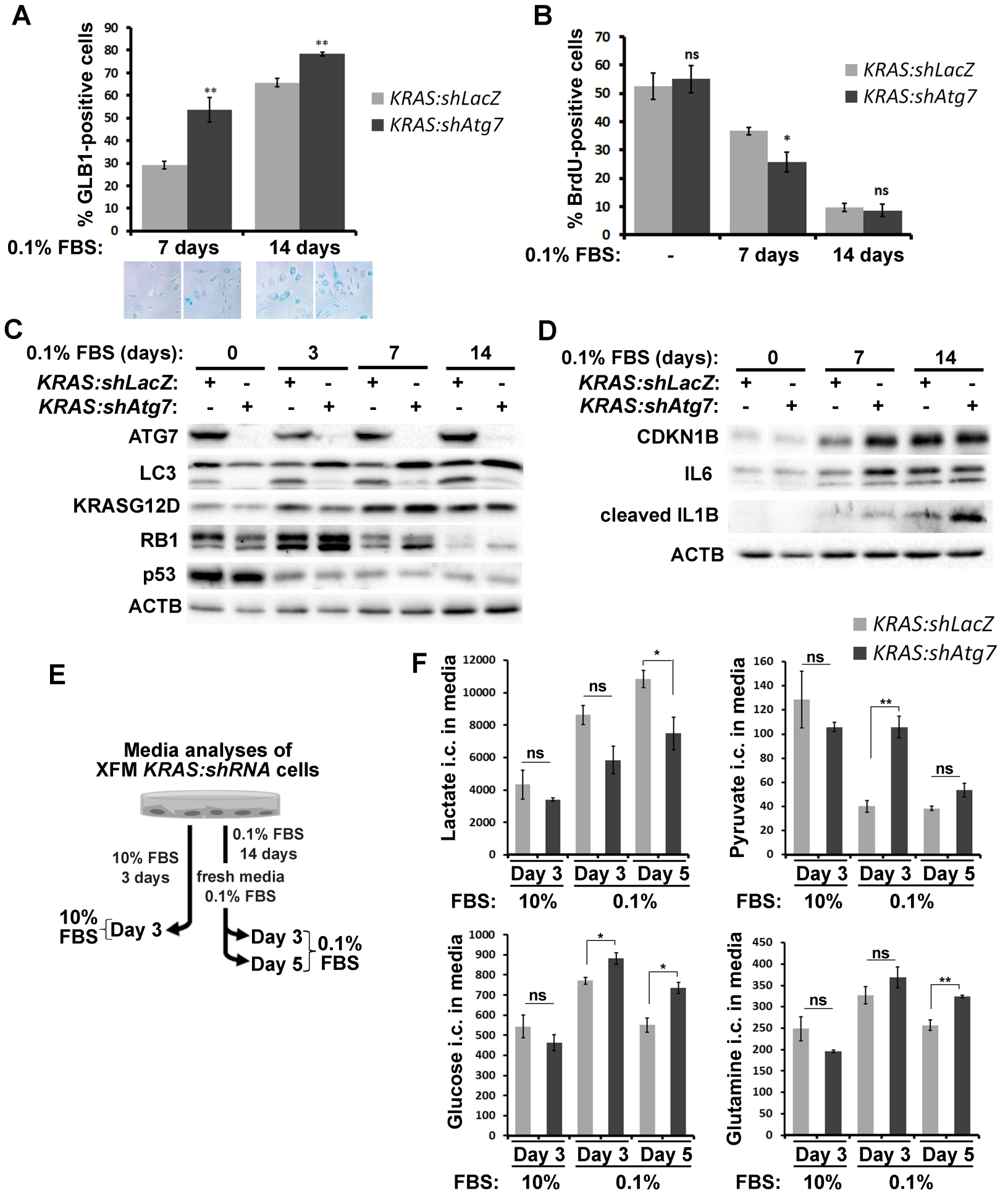
A
% GLB1-positive cells
KRAS:shLacZ
KRAS:shAtg7
0.1% FBS:
7 days
14 days
B
% BrdU-positive cells
KRAS:shLacZ
KRAS:shAtg7
0.1% FBS:
-
7 days
14 days
C
0.1% FBS (days):
KRAS:shLacZ:
KRAS:shAtg7:
ATG7
LC3
KRASG12D
RB1
p53
ACTB
D
0.1% FBS (days):
KRAS:shLacZ:
KRAS:shAtg7:
CDKN1B
IL6
cleaved IL1B
ACTB
E
Media analyses of
XFM KRAS:shRNA cells
10% FBS
3 days
0.1% FBS
14 days
fresh media
0.1% FBS
10% FBS
Day 3
Day 3
Day 5
0.1% FBS
F
KRAS:shLacZ
KRAS:shAtg7
Lactate i.c. in media
Pyruvate i.c. in media
Glucose i.c. in media
Glutamine i.c. in media
Day 3
Day 3
Day 5
FBS:
10%
0.1%